

Article

# Application of Pharmacokinetics Modelling to Predict Human Exposure of a Cationic Liposomal Subunit Antigen Vaccine System

Raj K. S. Badhan <sup>1</sup> , Swapnil Khadke <sup>2</sup> and Yvonne Perrie <sup>2,\*</sup>

<sup>1</sup> Aston Pharmacy School, School of Life and Health Sciences, Aston University, Birmingham B4 7ET, UK; r.k.s.badhan@aston.ac.uk

<sup>2</sup> Strathclyde Institute of Pharmacy and Biomedical Sciences, University of Strathclyde, Glasgow G4 0RE, UK; swapnil.khadke@strath.ac.uk

\* Correspondence: yvonne.perrie@strath.ac.uk; Tel.: +44-414-548-2244

Received: 16 October 2017; Accepted: 4 December 2017; Published: 7 December 2017

**Abstract:** The pharmacokinetics of a liposomal subunit antigen vaccine system composed of the cationic lipid dimethyldioctadecylammonium bromide (DDA) and the immunostimulatory agent trehalose 6,6-dibehenate (TDB) (8:1 molar ratio) combined with the Ag85B-ESAT-6 (H1) antigen were modelled using mouse in-vivo data. Compartment modelling and physiologically based pharmacokinetics (PBPK) were used to predict the administration site (muscle) and target site (lymph) temporal concentration profiles and factors governing these. Initial estimates using compartmental modelling established that quadriceps pharmacokinetics for the liposome demonstrated a long half-life (22.6 days) compared to the associated antigen (2.62 days). A mouse minimal-PBPK model was developed and successfully predicted quadriceps liposome and antigen pharmacokinetics. Predictions for the popliteal lymph node (PLN) aligned well at earlier time-points. A local sensitivity analysis highlighted that the predicted  $AUC_{\text{muscle}}$  was sensitive to the antigen degradation constant  $k_{\text{deg}}$  (resulting in a 3-log change) more so than the fraction escaping the quadriceps ( $f_e$ ) (resulting in a 10-fold change), and the predicted  $AUC_{\text{PLN}}$  was highly sensitive to  $f_e$ . A global sensitivity analysis of the antigen in the muscle demonstrated that model predictions were within the 50th percentile for predictions and showed acceptable fits. To further translate in-vitro data previously generated by our group, the mouse minimal-PBPK model was extrapolated to humans and predictions made for antigen pharmacokinetics in muscle and PLN. Global analysis demonstrated that both  $k_{\text{deg}}$  and  $f_e$  had a minimal impact on the resulting simulations in the muscle but a greater impact in the PLN. In summary, this study has predicted the in-vivo fate of DDA:TDB:H1 in humans and demonstrated the roles that formulation degradation and fraction escaping the depot site can play upon the overall depot effect within the site of administration.

**Keywords:** pharmacokinetics; physiologically based pharmacokinetics; liposome; antigen; adjuvant; vaccine

## 1. Introduction

The liposomal system composed of the cationic lipid dimethyldioctadecylammonium (DDA) and the immunomodulating glycolipid trehalose dibehenate (TDB) is a two-component adjuvant system known as CAF01. The CAF01 system has been shown to be effective in producing protective immune responses against pathogens such as chlamydia, malaria, influenza and tuberculosis (TB) [1,2]. Korsholm et al. (2007) described that one of the key mechanisms behind this immunomodulatory effect results from the cationic charge of the vesicles, which electrostatically binds and enhances antigen uptake by antigen-presenting cells via actin-dependent endocytosis [3]. This action works in synergy

with the immunostimulation provided by TDB; TDB is a synthetic analog of trehalose 6-6-dimycolate, an immunostimulatory component of *Mycobacterium tuberculosis*, a mycelium-recognised ligand and its adjuvant effect in vivo is MyD88 dependent [4].

When considering the biodistribution of these cationic liposomal adjuvants after immunisation, research from our group has shown that DDA:TDB liposomes are retained at the injection site and that these vesicles promote the retention of antigen at the site of injection, thus promoting co-delivery of both liposomal adjuvant and antigen to appropriate antigen-presenting cells [5]. A stable and reproducible dual-radiolabelling method (whereby the adjuvant (liposome) is labelled with  $^3\text{H}$  and the antigen (a subunit protein) with  $^{125}\text{I}$ ) was used to track liposomes and antigen in vivo [6]. The depot effect was found to be dependent on the cationic nature of vesicles; when DDA was replaced with neutral lipid distearyl phosphatidylcholine (DSPC), no depot was formed at site of injection and lower levels of immune responses were noted [7]. It has also been shown that DDA:TDB vesicles from ~200 to 1500 nm have similar clearance kinetics from the injection site. This suggests that with these cationic systems, size reduction does not modify clearance kinetics [8]. This could be a result of aggregation of these cationic liposomes after injection. Furthermore, whilst not modifying the clearance rates of the vesicles, the presence of TDB within the liposomes promotes increased recruitment of monocytes to the depot, again demonstrating the synergistic delivery and stimulatory action of the DDA:TDB formulation [5]. However, clearance rates from the injection site can be increased by PEGylation of these cationic liposomes [9,10]. Due to the hydrophilic chains of the polyethylene glycol (PEG) extending out from the surface of the liposomes, the cationic charge of the DDA is masked and hence aggregation is blocked [9]. This results in a faster drainage of the liposomes from the site of injection compared to non-PEGylated liposomes [9,10].

Despite these recognised links between distribution profiles and vaccine efficacy, the application of pharmacokinetic modelling and simulation to vaccines is sparse. This often results from a lack of understanding of how traditional pharmacokinetic terms developed for low molecular weight agents can be correlated to antigen dose, safety and efficacy, and is supported by a lack of appropriate correlations to efficacy. A complete understanding of the pharmacokinetics of liposomal formulations is limited, and modelling approaches to support formulation development is still in its infancy as a discipline. However, recently, a number of groups have begun to develop mechanisms by which to understand these processes in the context of pharmacokinetic modelling and simulation [11–17]. Whilst the pharmacokinetics of the Ag85B-ESAT antigen has not been assessed in humans, a liposome formulation with the antigen has undergone phase-1 trials demonstrating safety and tolerability [18,19]. The purpose of this study was to explore the potential to apply the principles of pharmacokinetic modelling and simulation to the analysis of the kinetics of liposome–antigen disposition data generated in mice through traditional compartmental modelling and physiologically based pharmacokinetics (in humans).

## 2. Materials and Methods

### 2.1. Data Collection

Data previously generated by our group from a dual radio-labelled DDA:TDB liposome–adjuvant (Ag85B-ESAT-6) formulation [9,20–22] was used for these pharmacokinetics studies. Biodistribution data obtained from these previous studies was used as either relative to the percent dosed or converted to mass units (300  $\mu\text{g}$  liposome and 2  $\mu\text{g}$  antigen) for dosing. During these studies from which the data was used, radio-labelled antigen and liposomes were used as previously outlined [6]. Briefly, the antigen was radio-labelled with  $^{125}\text{I}$  using Pierce iodination tubes containing Pierce iodination reagent. The tubes contain an oxidizing reagent which converts NaI into a reactive iodine molecule that can insert into the tyrosol group of tyrosine amino acids. Liposomes were radio-labelled using commercially available tritiated lipid dipalmitoyl phosphatidylcholine (DPPC). Addition of this tracer lipid did not affect the physicochemical properties of DDA:TDB. Liposome membrane stability

and retention of the radiolabel tracer upon exposure of liposomes to the in-vivo environment was previously confirmed using stability studies at 37 °C in a high-protein environment (50% Fetal Calf Serum (FCS)) [5]. Mice were injected with Ag85BESAT-6 (radiolabeled with <sup>125</sup>I)-adsorbing liposome (radiolabeled with <sup>3</sup>H) formulations (50 µL/dose, im (intramuscular) injection). At 1, 4 and 14 days post-injection (pi), mice were terminated by cervical dislocation and tissue from the site of injection (SOI), and local draining lymph nodes (LNs) were removed for analysis of liposome (<sup>3</sup>H) and antigen (<sup>125</sup>I) using methods previously described elsewhere [6].

In the studies where the in-vivo data were used in the modelling, liposomes were composed of DDA:TDB at a weight ratio of 5:1. Mice received 50 µL/dose which contained 250 µg DDA, 50 µg TDB and 2 µg of antigen. Liposomes were in the range of 400 to 600 nm in size (z-average diameter of 481 ± 20 with a PDI of 0.23 ± 0.1) and highly cationic in nature (55 to 65 mV).

## 2.2. Compartmental Modelling of Data

A 1-, 2- and 3-compartment model (Figure 1) was used to fit the data for the liposome and antigen to model the kinetics at the site of administration (central compartment). Differential equations described a 1-, 2- and 3-compartment model and were numerically solved using Matlab (The MathWorks Inc., Natick, MA, USA, 2015):

1-compartment model:

$$\frac{dC_1}{dt} = -k_{10} \cdot C_1; \quad (1)$$

2-compartment model:

$$\frac{dC_1}{dt} = -(k_{10} + k_{12}) \cdot C_1 + k_{21} \cdot C_2; \quad (2)$$

$$\frac{dC_2}{dt} = k_{12} \cdot C_1 - k_{21} \cdot C_2; \quad (3)$$

3-compartment model:

$$\frac{dC_1}{dt} = -(k_{10} + k_{12} + k_{13}) \cdot C_1 + k_{21} \cdot C_2 + k_{31} \cdot C_3; \quad (4)$$

$$\frac{dC_2}{dt} = k_{12} \cdot C_1 - k_{21} \cdot C_2; \quad (5)$$

$$\frac{dC_3}{dt} = k_{13} \cdot C_1 - k_{31} \cdot C_3; \quad (6)$$

where  $C_n$ : concentration in nth compartment; t: time;  $k_{10}$ : elimination rate constant;  $k_{12}$ : transfer rate constant from central (1) to peripheral (2) compartment;  $k_{21}$ : transfer rate constant from peripheral (2) to central (1) compartment;  $k_{13}$ : transfer rate constant from central (1) to peripheral (3) compartment;  $k_{31}$ : transfer rate constant from peripheral (3) to central (1) compartment.

Pharmacokinetics parameters were then calculated based on the best-fitting model selected according to the Akaike information criterion (AIC).

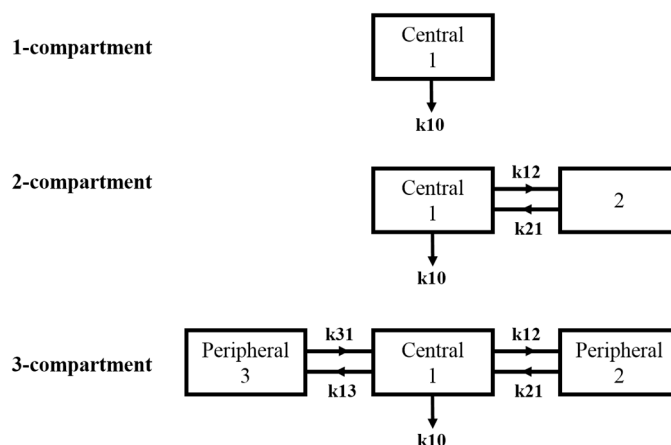


**Figure 1.** Schematic diagram of compartmental model. Boxes represent non-physiological compartments within which the drug is capable of distributing. Arrows indicate direction of transfer between compartments with 'k' indicating a transfer rate constant and the numerals indicating the direction of transport.  $k_{10}$  reflects degradation from a compartment.

### 2.3. Mechanistic Modelling of Data

Minimal-PBPK (physiologically based pharmacokinetics) models of mice (28 g) and humans (71 kg) [23] were developed and accounted for the site of injection (muscles), target site (PLN), rest of body (ROB) and plasma (Figure 2). Compartments were assigned physiological volume parameters and connected through physiological flows (Table 1). A more mechanistic model, with the inclusion of, for example, a tissue partition coefficient, was not developed due to the lack of rich sampling data points to develop/validate the model with.

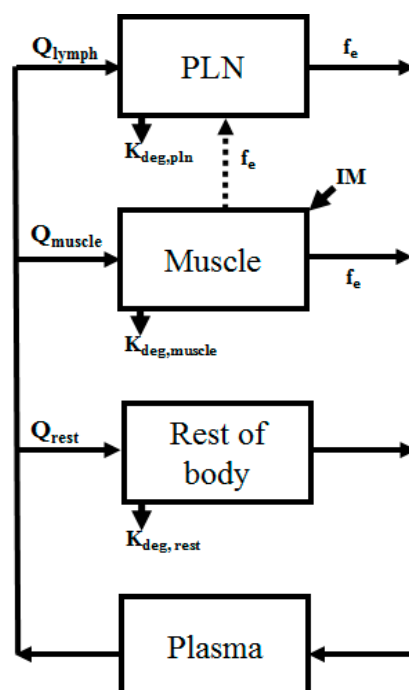


**Figure 2.** Schematic represent of the semi-mechanistic PBPK model. Arrows indicate flow between organs. Dashed lines indicates lymphatic drainage. IM: intramuscular administration.

**Table 1.** Anatomic and physiological parameters used in the physiologically based pharmacokinetics (PBPK) models; PLN: popliteal lymph node <sup>1</sup>.

Compartment	Flow (L/Day) Symbol	Mouse	Human	Volume (L) Symbol	Mouse	Human
Plasma	$Q_{\text{plasma}}$	-	-	$V_{\text{plasma}}$	$9.44 \times 10^{-4}$ [24]	3.13
Quadriceps	$Q_{\text{muscle}}$	2.60 [24]	32.04 [25]	$V_{\text{muscle}}$	$1.6 \times 10^{-4}$ [26]	0.19 [25]
PLN	$Q_{\text{PLN}}$	$2 \times 10^{-3}$ [27]	0.52 [27]	$V_{\text{PLN}}$	$5 \times 10^{-6}$ [26]	$3.5 \times 10^{-3}$ [27]
Rest of Body	$Q_{\text{rest}}$	18.10	$3.02 \times 10^4$	$V_{\text{rest}}$	$2.6 \times 10^{-2}$	67.68

<sup>1</sup> Except where indicated, all parameters were taken from [23].

The following assumptions were made for this model:

- All tissues were modelled based on the total tissue volume (derived from tissue mass), and, where necessary, assuming a density of 1.
- The ‘muscle’ compartment was modeled solely by the quadriceps tissue component in mice and the deltoid tissue in humans.
- The ‘lymph’ compartment was modelled solely by the popliteal lymph node (PLN) with an estimated whole tissue volume of 0.05 mL [28] (assuming a density = 1) in mice. In humans we assumed a mass of 0.05 g/kg body weight, based on a similar relationship in rabbits [27].
- Plasma flow to and drainage from the PLN were assumed to be 0.012% cardiac output [27].
- The fraction escaping ( $f_e$ ) the quadriceps and being drained into the PLN was fixed at  $3 \times 10^{-5}$  for liposome and  $3.6 \times 10^{-6}$  for antigen, to reflect fraction escaping the muscle based upon the average ratio of percent accumulation for all time points in the target tissues compared to the dose administered. The small-pore theory of molecular translocation across a membrane would preclude molecules below 60 nm in size from undergoing transvascular flow across a capillary wall [29–32].
- Dosing was modelled as a rapid first-order dose into the quadriceps (approximating a bolus dose) with a  $k_a = 10 \text{ day}^{-1}$ . The human model focused on simulating antigen only and therefore a human dose of 50  $\mu\text{g}$  was modelled.
- In the absence of plasma concentration of both liposome and antigen and the limited muscle and PLN biodistribution data, an attempt to estimate an appropriate tissue partition coefficient was not conducted and transfer of liposome/antigen out of the site of administration was assumed to occur only through exiting via the muscle blood flow (accounting for the fraction escaping) and the transfer via lymphatics. Transvascular flow was therefore modelled as a rate constant (when accounting for tissue volume):

$$tv_{\text{tissue}} = \frac{Q_{\text{tissue}} f_e}{V_{\text{tissue}}}$$

Differential equations describing the drug flow in the model were solved in Matlab (The MathWorks Inc., Natick, MA, USA, 2015) and are detailed as follows:

Plasma:

$$V_{\text{plasma}} \cdot \frac{dA_{\text{plasma}}}{dt} = -(\sum Q_{\text{tissue}}) \cdot C_{\text{plasma}} + (Q_{\text{rest}} \cdot C_{\text{rest}}) + (tv_{\text{muscle}} \cdot C_{\text{muscle}}) + (tv_{\text{lymph}} \cdot C_{\text{PLN}}). \quad (7)$$

ROB:

$$V_{\text{rest}} \cdot \frac{dA_{\text{rest}}}{dt} = -((Q_{\text{rest}} \cdot C_{\text{rest}}) + (k_{\text{deg,rest}} \cdot C_{\text{rest}})) + (Q_{\text{rest}} \cdot C_{\text{plasma}}). \quad (8)$$

Quadriceps:

$$V_{\text{muscle}} \cdot \frac{dA_{\text{muscle}}}{dt} = ka \cdot \text{Dose} - \left( (tv_{\text{muscle}} \cdot C_{\text{muscle}}) + (k_{\text{deg,muscle}} \cdot C_{\text{muscle}}) + (tv_{\text{lymph}} \cdot C_{\text{muscle}}) \right) + (Q_{\text{muscle}} \cdot C_{\text{plasma}}) \quad (9)$$

PLN:

$$V_{\text{PLN}} \cdot \frac{dA_{\text{PLN}}}{dt} = - \left( (tv_{\text{lymph}} \cdot C_{\text{PLN}}) + (k_{\text{deg,PLN}} \cdot C_{\text{PLN}}) \right) + (Q_{\text{PLN}} \cdot C_{\text{plasma}}) + (tv_{\text{lymph}} \cdot C_{\text{muscle}}) \quad (10)$$

Given the lack of robust plasma and whole-body temporal concentration data, parameter optimisation was initially avoided as far as possible, except for the optimisation of the degradation rate constant of the formulation from each tissue ( $k_{\text{deg,tissue}}$ ). Optimisation was conducted using a non-linear least-squares fitting algorithm based on previously reported data. Final model simulations were confirmed through visual inspection and observed versus predicted plots (for mouse model only). The percent predictive error (PE) was calculated (see Equation (11)) for mouse data only, where  $C_{\text{pred}}$  is the model-predicted concentration and  $C_{\text{obs}}$  the observed concentration:

$$\% \text{ PE} = \frac{C_{\text{pred}} - C_{\text{obs}}}{C_{\text{obs}}} \times 100\% \quad (11)$$

#### 2.4. Parameter Sensitivity Analysis

An uncertainty analysis was performed to determine how variations in model parameters would influence the depot effect in the target site (muscle) for the mouse model only. A local analysis was performed on  $Q_{\text{muscle}}$ ,  $k_{\text{deg}}$  and  $f_e$ , and was scanned over a defined range ( $Q_{\text{muscle}}$ :  $\pm 3$ -log;  $k_{\text{deg}}$ :  $\pm 3$ -log and  $f_e$ :  $\pm 4$ -log). 3D surface plots of the relationship between two input parameters and the  $AUC_{\text{muscle}}$  were compared in the muscle and the PLN.

A global analysis was also conducted on muscle kinetics for the liposome and antigen, with scanning limits set as detailed above. Monte Carlo simulations with 1000 simulations were performed with the Latin hypercube sampling algorithm for both the mouse and human models. The resultant 50th and 95th percentiles were graphically assessed.

### 3. Results

#### 3.1. Compartment Modelling

The pharmacokinetics of the liposome formulation was best described by a 1-compartment model with antigen described by a 2-compartment model (Figure 3). Antigen stability was described by fitting in-vitro stability data to a bi-exponential first-order degradation model (Figure 4), demonstrating a terminal half-life of 2.62 days and relatively slow degradation rate of  $0.34 \text{ day}^{-1}$  (Table 2).

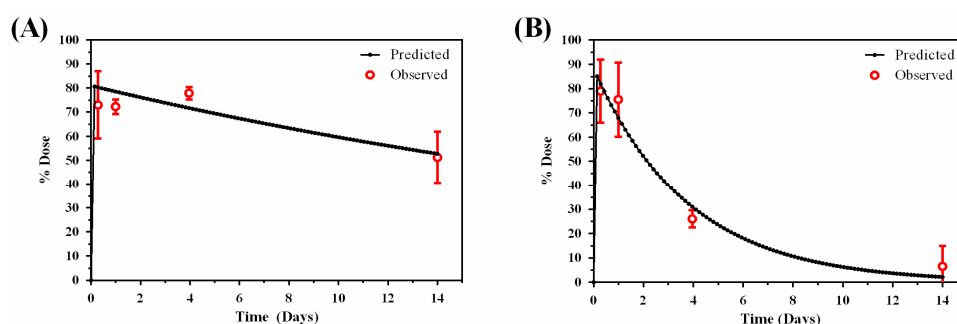
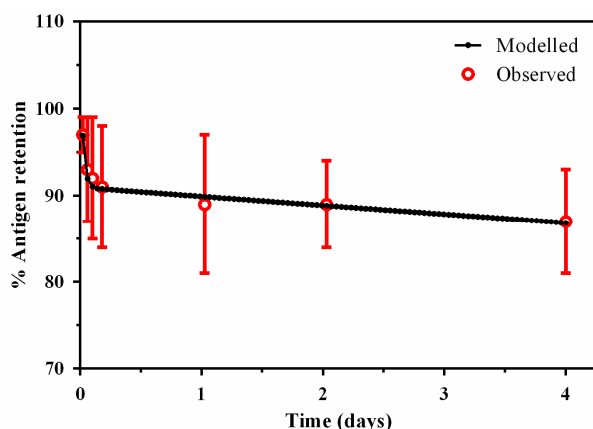


Figure 3. Compartmental modelling estimates for: (A) liposome and (B) antigen at the muscle.



**Figure 4.** A bi-exponential model of in-vitro antigen stability.

**Table 2.** Summary of model-fitted pharmacokinetic parameters.

Liposome	
K10	0.0306 day <sup>-1</sup>
t <sub>1/2</sub>	22.6 days
MRT	32.6 days
AIC	49.54
Antigen	
k10	0.34 day <sup>-1</sup>
k12	22.26 day <sup>-1</sup>
k21	77.58 day <sup>-1</sup>
t <sub>1/2α</sub>	0.0069 day
t <sub>1/2β</sub>	2.62 days
MRT	3.78 days
AIC	37.4

Parameters best fit a 1-compartment model for the liposome and a 2-compartment model for the antigen. MRT: mean residence time; t<sub>1/2α</sub>: distribution half-life; t<sub>1/2β</sub>: terminal half-life; AIC: Akaike information criterion.

### 3.2. Minimal-PBPK Models

We first aimed at developing a physiological model which best mimicked the kinetics of distributional transfer and degradation kinetics of the formulation at the key target site, namely the muscle. This was further followed on by assessing the ability to predict drainage of the formulation into the local lymph node, that is, the PLN. Modelling was generally deemed to be successful, particularly for the muscle and for both the liposome and antigen. The PBPK model developed was able to capture the kinetics within the compartment with a PE < 33% for the liposome (Figure 5A,B and Table 3). For the antigen, the precision PE was less than 14% for time points 1–4 days, with the final time point showing a larger error (65.9%) (Figure 5C,D and Table 2). In a similar fashion the PLN predictions were also generally successful but demonstrated poorer predictions at 14 days. Fitting of the degradation rate constants yielded estimates that were similar to those from compartment modelling and in-vitro data (Table 4), with antigen demonstrating on average a 10-fold higher rate constant than liposomes.

**Table 3.** Precision error calculations.

Time (Days)	% Precision Error			
	Muscle		PLN	
	Liposome	Antigen	Liposome	Antigen
0.25	16.4	13.5	-	-
1	32.7	5.3	28.4	32.7
4	3.9	13.8	13.90	41.5
14	3.8	65.9	66.3	74.0

Table 4. Parameter estimates for  $k_{deg}$ .

Compartment	Degradation Constant ( $\text{Day}^{-1} \pm \text{SD}$ )		
	Symbol	Liposome	Antigen
Plasma	-	-	-
Quadriceps	$k_{deg,muscle}$	$0.051 \pm 0.008$	$0.320 \pm 0.028$
PLN	$k_{deg,pln}$	$0.132 \pm 0.004$	$0.280 \pm 0.013$
Rest of Body	$k_{deg,rest}$	$0.091 \pm 0.040$	$0.110 \pm 0.030$

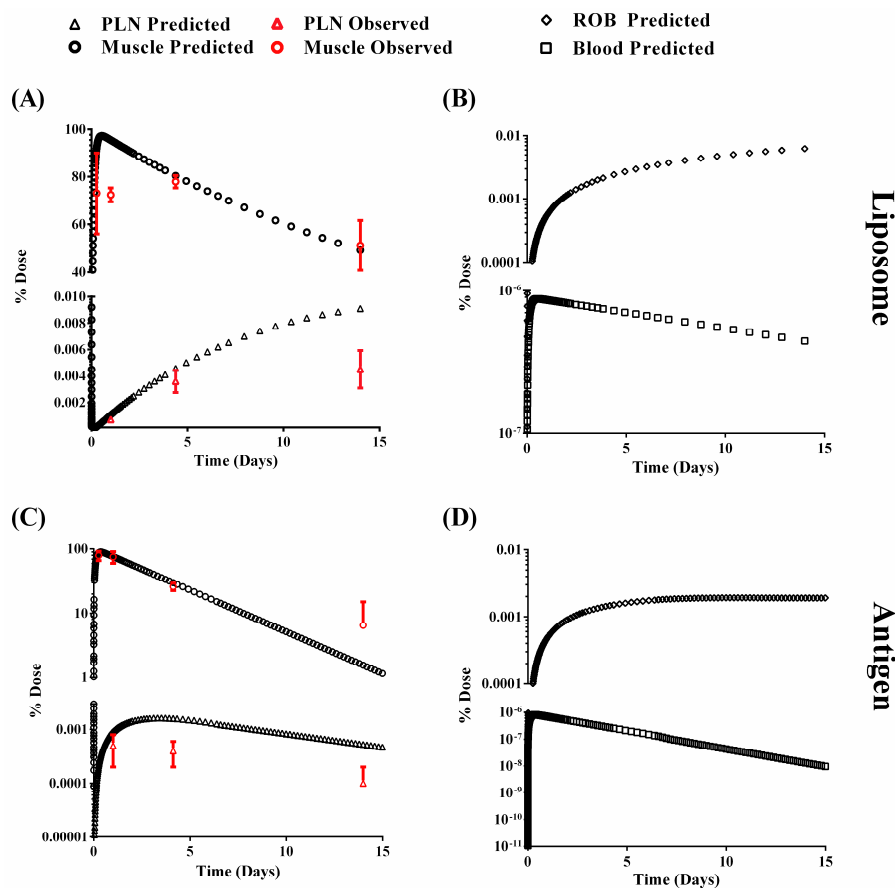


Figure 5. PBPK model predictions for liposome (A,B) and antigen (C,D). Muscle and PLN data is shown in (A,C), and blood and ROB in (B,D). Red data points represent observed data.

### 3.3. Sensitivity Analysis

In light of sparse observed data sets, the sensitivity of model input parameters was evaluated through both global and local sensitivity analyses. Local sensitivity analysis was conducted on  $k_{deg}$ ,  $f_e$ ,  $Q_{muscle}$  and  $Q_{lymph}$ , where the impact of two of these parameters on  $AUC_{tissue}$  was assessed. Analysis was conducted with both liposomes and antigen, with similar trends in sensitivities and therefore liposome trends reported in Figure 6.

The analysis revealed that the  $AUC_{muscle}$  was most sensitive to  $k_{deg,muscle}$  (Figure 6A), leading to a 2-log magnitude change in  $AUC_{muscle}$  over the  $k_{deg,muscle}$  range studied ( $0.001$ – $10 \text{ day}^{-1}$ ), and more particularly beyond  $0.1 \text{ day}^{-1}$ . Our model-fitted estimate for  $k_{deg,muscle}$  was at the lower end of this sensitivity.  $AUC_{muscle}$  was also highly sensitive to changes in  $f_e$ , with  $Q_{muscle}$  not impacting upon the sensitivity of  $AUC_{muscle}$  (Figure 6B).

$AUC_{PLN}$  was most sensitive to changes in  $f_e$ , with an almost 8-log-order change in  $AUC_{lymph}$  over the range of  $f_e$  studied (Figure 6C).  $Q_{lymph}$  and  $k_{deg,pln}$  also resulted in some level of sensitivity on

$AUC_{lymph}$  (Figure 6C), however, our estimates for  $k_{deg,pln}$  are at the upper limit of the sensitivity of the parameters towards  $AUC$  and  $Q_{lymph}$  in the mid-range, but in both cases a 50% change in parameter would still provide an estimate of  $AUC_{lymph}$  within the same order of magnitude (Figure 6D).

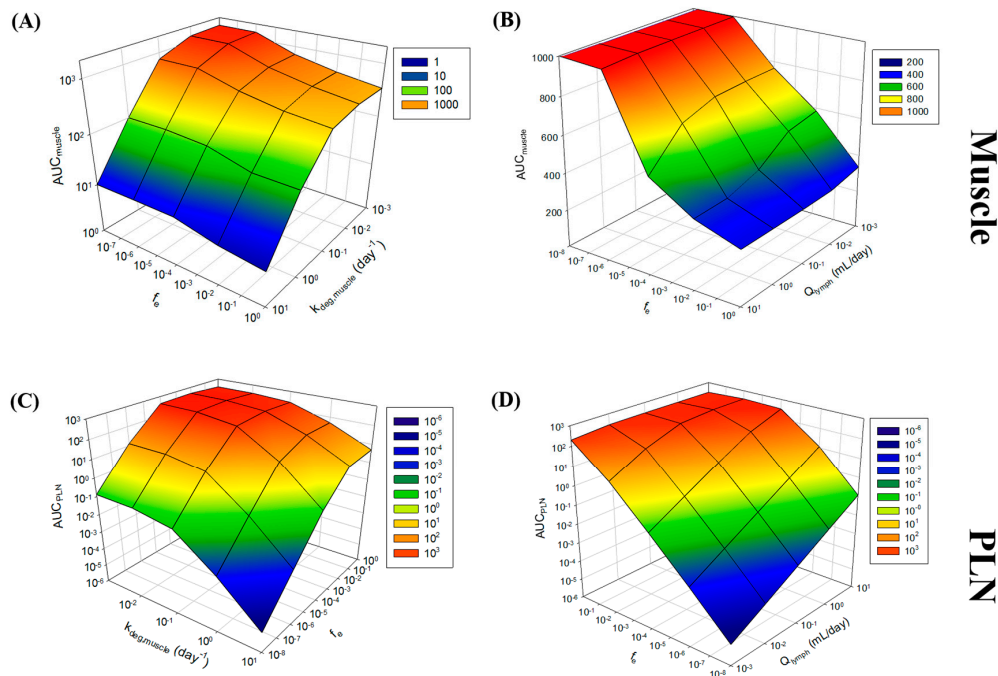


**Figure 6.** Local sensitivity analysis of  $f_e$ ,  $k_{deg}$ ,  $Q_{muscle}$  and  $Q_{lymph}$  towards  $AUC_{muscle}$  (A,B) or  $AUC_{PLN}$  (C,D). Note the differences in the z-axis scales.

As a result of these local simulations,  $k_{deg,muscle}$  and  $f_e$  were selected for global analysis in the muscle for the antigen (Figure 7). The global analysis revealed a limited uncertainty in the predictions at the earlier time-points for  $k_{deg,muscle}$  (Figure 7A), with the uncertainty increasing later in the simulation. With  $f_e$ , sensitivity analysis revealed no impact on predictions with very low  $f_e$  ( $<1 \times 10^{-5}$ ) (Figure 7B), but when  $f_e$  was increased above  $1 \times 10^{-5}$ , the uncertainty around the  $C_{max}$  increased significantly (Figure 7C) and impacted more on the earlier time points ( $<6$  days).

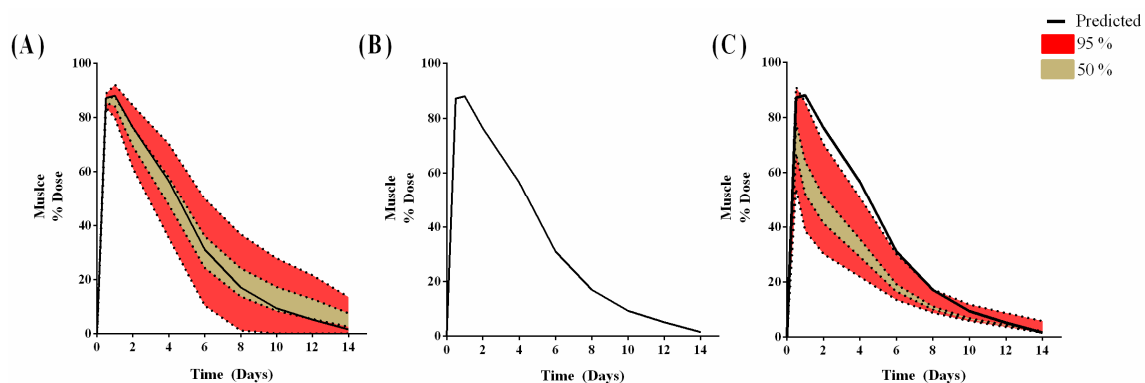


**Figure 7.** The uncertainty in the antigen muscle concentrations, following 1000 model simulations with a 3-fold change in  $k_{deg,muscle}$  (A);  $1 \times 10^{-8}$  to  $1 \times 10^{-5}$  change in  $f_e$  (B) and  $1 \times 10^{-5}$  to  $1 \times 10^{-1}$  change in  $f_e$  (C) was simulated. The solid line represents PBPK-predicted profiles.

### 3.4. Human Model

The mouse model was extrapolated to develop a human PBPK model for the antigen only with the dose adjusted to reflect a single dose administered in adults (i.e., 50  $\mu\text{g}$ ). In the muscle, the predicted  $C_{\text{max}}$  was 0.25  $\mu\text{g}/\text{mL}$  with a  $t_{\text{max}}$  of 0.5 days and half-life of 13.2 days (Figure 8A,B). In the PLN the predicted  $C_{\text{max}}$  was 0.0438  $\mu\text{g}/\text{mL}$  with a  $t_{\text{max}}$  of 2 days and half-life of 13.2 days (Figure 8C,D). A global sensitivity analysis was then conducted to compare  $k_{\text{deg,tissue}}$  and  $f_e$  on muscle and PLN concentration. Uncertainty in the predictions on antigen concentration in the muscle with variation of  $k_{\text{deg}}$  ( $\pm 50\%$ ) was minimal at the earlier time point, but became more uncertain during the simulations (Figure 8A).

For variations in  $f_e$ , the antigen concentration in the muscle was not sensitive to any change over the range of  $1e^{-8}$  to  $1e^{-5}$  (Figure 8B-insert). However, for the range of  $1 \times 10^{-5}$  to  $1 \times 10^{-1}$ , muscle antigen concentration demonstrated minimal sensitivity and predictions were within the upper 95th percentile (Figure 8B). For the PLN, this uncertainty was significantly greater and predictions were within the lower 95th percentile range for both  $k_{\text{deg}}$  (Figure 8C) and  $f_e$  (Figure 8D).

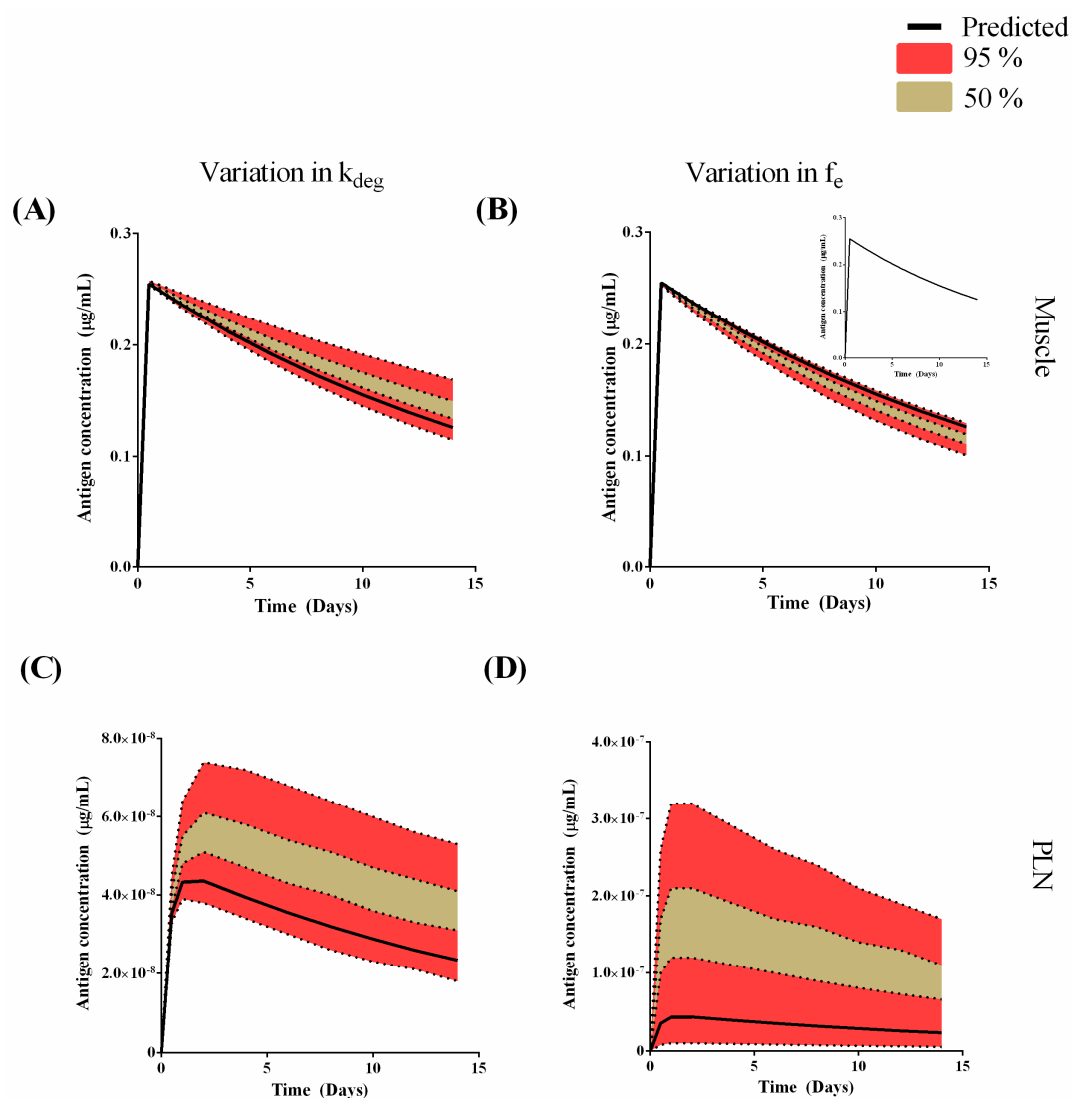


**Figure 8.** Model predictions (black solid line) and global sensitivity analysis for muscle (A,B) and PLN (C,D). (A,C) show a  $\pm 50\%$  variation in  $k_{\text{deg}}$ ; (B-insert) and (D) show a variation in  $f_e$  from  $1 \times 10^{-8}$ – $1 \times 10^{-5}$ ; (B) shows a variation in  $f_e$  from  $1 \times 10^{-5}$ – $1 \times 10^{-1}$ .

## 4. Discussion

Vaccination plays a key role in the protection of life and promotion of global public health. The use of liposomal vaccine adjuvants offers new approaches to take advantage of the immunomodulatory properties imparted by these systems. This study has focused on demonstrating how mathematical modelling, in the form of pharmacokinetics modelling and simulation, can be applied to gain an early perception of the pharmacokinetic properties of formulation systems for vaccines and adjuvants.

### 4.1. Compartmental Modelling

Compartmental modelling is a widely used empirical tool which can be used to quantify the pharmacokinetics of a molecule of interest from existing data. It makes the assumption that drug distributes instantaneously within a compartment and that the central compartment is often assumed to be the dosing or 'plasma' compartment. Compartment modelling in this context models the kinetics within the dosing (quadriceps muscle) compartment in an attempt to describe the pharmacokinetics of both the liposome and the associated antigen.

Compartment modelling demonstrated that the liposome is indeed relatively stable and resides at the site of injection. The antigen on the other hand yielded a 10-fold higher elimination rate ( $k_{10}$ ) compared to the liposome (Table 2). As  $k_{10}$  is traditionally viewed as an 'elimination' process, in this context it can be related to processes driving the reduction of liposome from the dosing compartment. The higher  $k_{10}$  for antigen may suggest either a more-rapid degradation process within the muscle tissue or more-rapid transfer out of the injection site. A significant drawback of compartmental modelling is highlighted in this approach, as it is difficult to assign biochemical or physiological processes to the rate constants that define the compartmental transfer of the formulation. This can include uptake by antigen-presenting cells, which will take up and clear the vaccine from the injection site. Our analysis of the reported in-vitro stability of antigen demonstrates that the antigen was relatively stable in vitro (in the absence of enzymatic degradation processes), with a degradation rate of  $0.01 \text{ day}^{-1}$ . This demonstrates a relatively slow degradation process and leads to a long terminal half-life of approximately 60 days. A key drawback of compartmental modelling is the inability to extrapolate to other species (e.g., humans) and other types of formulations as the very structure of the model is intricately tied up, and its empirical nature requires in-vivo data to model.

### 4.2. Physiological Modelling

Physiologically based pharmacokinetics (PBPK) is an adaptation of compartmental modelling, where the system is described in the context of physiological and biochemical properties, that is, tissue volumes, blood flows and protein/enzymatic expression. We opted to develop a minimal-PBPK model; a model that is semi-physiological and which accounts for the key processes governing formulation disposition at the site of administration and target tissues. Our rationale for choosing this approach, as opposed to a full implementation of a whole-body PBPK model, was driven by: (i) the sparse data available from existing studies for our formulation of choice; (ii) the lack of plasma data which is important when developing a whole-body PBPK model; and (iii) the desire to avoid fitting a large majority of model parameters where the final estimates would undoubtedly be unreliable due to the limited available data.

Our approach developed four compartmental models consisting of blood, rest of body, muscle and popliteal lymph node (PLN) sites (Figure 2), with the site of administration being the muscle. Parameter estimation was only conducted for the degradation of liposomes or antigen at each tissue site. The initial model estimates of the liposomes in the muscle were relatively good, with the exception of the fit at day one (PE = 32.7%), with a similar trend for the liposome in the PLN, with good fits to observed data except for day 14 (PE = 66.3%) (Table 2). The large variability in the 0.25-day observed sampling point and poorer fit at day one may suggest non-uniform tissue distribution following injection. However, the lack of plasma data precluded further analysis of this to ascertain why there is

this mismatch. In a similar fashion, the poor fit at days 14 in the PLN would suggest an alternative competing process resulting in the slower penetration into the tissue (Figure 5A). Yet, given the limited data points, this first approach at modelling the kinetics of liposome distribution from muscle into PLN is relatively successful. Indeed, the dose reaching the blood was significantly lower ( $<1 \times 10^{-6}\%$  of the administered dose) and highlights the expected depot effect the muscle provides in maintaining the formulation within the dosing tissue.

For the antigen, we were able to describe the muscle kinetics relatively well with a higher PE at days 14 (65.9%) (Figure 5A and Table 2). Our model prediction for the PLN was predominately within the same order as magnitude as the reported data but with a higher PE than the muscle compartment. Given these concerns, we conducted a local sensitivity analysis to better identify parameters that lead to sensitivity to the residence of drug within the muscle and PLN (Figure 6). Both  $k_{\text{deg,muscle}}$  and  $f_e$  resulted in sensitivity towards  $\text{AUC}_{\text{muscle}}$  (Figure 6A), with  $k_{\text{deg,muscle}}$  being the most sensitive to changes in  $\text{AUC}_{\text{muscle}}$ . This suggests that  $f_e$  only plays a minor role in governing the residency of the formulation within the muscle. For example, an 8-fold log change in  $f_e$  at a fixed  $k_{\text{deg,muscle}}$  of  $0.051 \text{ day}^{-1}$  resulted in 2-fold change in  $\text{AUC}_{\text{muscle}}$  (Figure 6A), whereas a fixed  $f_e$  utilised within the model resulted in a 3-log change in  $\text{AUC}_{\text{muscle}}$  over the range of  $k_{\text{deg,muscle}}$  simulated.

In the PLN, both  $f_e$  and  $k_{\text{deg,pln}}$  were able to affect AUC, with changes in  $f_e$  again being more prominent in influencing  $\text{AUC}_{\text{PLN}}$  (Figure 6C,D). At a  $f_e = 1$ ,  $\text{AUC}_{\text{PLN}}$  is less sensitive to changes in  $k_{\text{deg,pln}}$  (Figure 6C), presumably as a result of the unhindered formulation flux between compartments. However, when fixed at  $1 \times 10^{-8}$ ,  $k_{\text{deg,pln}}$  resulted in a 5-fold change in  $\text{AUC}_{\text{PLN}}$  and became more important in controlling  $\text{AUC}_{\text{PLN}}$ .

The local analysis has revealed the need to further quantify the 'degradation' process (i.e., antigen processing pathways: uptake, degradation, complex formation and presentation) to improve the sensitivity of the model to changes (estimates) for  $k_{\text{deg,tissue}}$  and  $f_e$ . A more mechanistic approach to describe these pathways may better capture the kinetics events associated with  $k_{\text{deg,tissue}}$ . In particular, when considering a global sensitivity analysis (Figure 7), with respect to the impact of both  $k_{\text{deg,muscle}}$  (Figure 7A) and  $f_e$  (Figure 7B) on percent dose, our predictions are within the 50th and 95th percentile in the muscle, but there is more uncertainty in the PLN, where a significantly wider range for the 95th percentile exists. This, coupled with the relatively low recovery, may require further studies to better characterise the reasons for such low accumulation (if it cannot be attributed to the size and impact on  $f_e$ ).

When extrapolating our model to humans, we have obtained first estimates of the potential injection site concentration (Figure 8) with a predicted mean  $C_{\text{max}}$  of  $0.25 \mu\text{g}/\text{mL}$  and long half-life of 13.2 days in the deltoid muscle. This half-life is shorter than that predicted in the mouse quadriceps. The degradation of the antigen appears to have a more prominent role in governing its residency within the muscle (Figure 8A) rather than its ability to be cleared from the muscle tissue (Figure 8B). This may reflect the size of the liposomes (approximately 500 nm and highly cationic in nature) and their ability to be cleared from the depot site. Our approach to utilise percent-recovery data is a suitable first approximation at determining a static true 'in-vivo' parameter, particularly as the size of the nanoparticle would be expected to significantly hinder its drainage from the depot into the PLN and hence, our first-principals approach is justified.

In summary, this study has demonstrated the potential to apply the principles of pharmacokinetics to assess in-vivo data from liposome studies, but also shows how we can apply pharmacokinetics in a mechanistic approach to allow cross-species extrapolation. It must be noted that caveats exist and should be considered when the reader wishes to apply pharmacokinetics principles to data sets.

Lack of plasma data: Key to any pharmacokinetics study is the requirement to sample from the blood/plasma. By sampling from the plasma (in addition to the target site), the reader is then able to take account of distributional processes to other tissues and hence move the model towards a more mechanistic full-PBPK model rather than the semi-mechanistic PBPK model presented in this study.

Interpretation of tissue partition: The passage of a therapeutic entity through a cell requires partitioning across cellular membranes. This is often accounted for by the tissue partition coefficient

(kp) [33,34], which can readily be predicted from the physiochemical properties of low molecular weight compounds. Our approach did not address this issue and assumed there was no inherent permeability barrier, with transvascular flux being the main factor governing the entry/exit to a tissue. Possessing prior knowledge of the formulation system, we surmised that the liposomes would be unable to partition out due to their size (~500 nm) and hence have focused on the depot effect provided by the muscle. For other nanoparticles, this may not be the case, and kps would need to be determined. By possessing plasma data along with some additional tissue data, it would be possible to obtain first estimates of the kp for each tissue of interest.

**Modelling antigen pharmacokinetics:** Our approach to the pharmacokinetic modelling of the antigen element of the formulation is simplistic when considering the multitude of processes involved in the absorption, distribution, metabolism and elimination (ADME) processing of the antigen, along with non-linear processes such as FcRn-mediated transcytosis and target site-mediated processes. A driving force for the selection of an appropriate model is the availability of data that support model development, and in this case we have presented a first-principles approach to capture some elements of the antigen pharmacokinetics.

## 5. Conclusions

In conclusion, this study showed an approach for predicting the in-vivo fate of DDA:TDB:H1 in humans and demonstrated the role that formulation degradation and fraction escaping the depot site can play in the overall depot effect within the site of administration.

**Acknowledgments:** This work was part funded by EU Horizon 2020 project TBVAC 2020 (Grant no. 643381) (Yvonne Perrie) and Aston University (Swapnil Khadke). The data supporting this paper can be accessed at <http://dx.doi.org/10.15129/88bbe99c-be63-4807-9b64-66a28aa18787>.

**Author Contributions:** Yvonne Perrie, Raj K. S. Badhan and Swapnil Khadke jointly conceived and designed the experiments, analyzed the data and wrote the paper.

**Conflicts of Interest:** The authors declare no conflict of interest.

## References

1. Agger, E.M.; Rosenkrands, I.; Hansen, J.; Brahimi, K.; Vandahl, B.S.; Aagaard, C.; Werninghaus, K.; Kirschning, C.; Lang, R.; Christensen, D.; et al. Cationic liposomes formulated with synthetic mycobacterial cordfactor (CAF01): A versatile adjuvant for vaccines with different immunological requirements. *PLoS ONE* **2008**, *3*, e3116. [[CrossRef](#)] [[PubMed](#)]
2. Holten-Andersen, L.; Doherty, T.M.; Korsholm, K.S.; Andersen, P. Combination of the Cationic Surfactant Dimethyl Dioctadecyl Ammonium Bromide and Synthetic Mycobacterial Cord Factor as an Efficient Adjuvant for Tuberculosis Subunit Vaccines. *Infect. Immun.* **2004**, *72*, 1608–1617. [[CrossRef](#)] [[PubMed](#)]
3. Korsholm, K.S.; Agger, E.M.; Foged, C.; Christensen, D.; Dietrich, J.; Andersen, C.S.; Geisler, C.; Andersen, P. The adjuvant mechanism of cationic dimethyldioctadecylammonium liposomes. *Immunology* **2007**, *121*, 216–226. [[CrossRef](#)] [[PubMed](#)]
4. Werninghaus, K.; Babiak, A.; Groß, O.; Hölscher, C.; Dietrich, H.; Agger, E.M.; Mages, J.; Mocsai, A.; Schoenen, H.; Finger, K.; et al. Adjuvanticity of a synthetic cord factor analogue for subunit Mycobacterium tuberculosis vaccination requires FcRgamma-Syk-Card9-dependent innate immune activation. *J. Exp. Med.* **2009**, *206*, 89–97. [[CrossRef](#)] [[PubMed](#)]
5. Henriksen-Lacey, M.; Bramwell, V.W.; Christensen, D.; Agger, E.-M.; Andersen, P.; Perrie, Y. Liposomes based on dimethyldioctadecylammonium promote a depot effect and enhance immunogenicity of soluble antigen. *J. Control. Release* **2010**, *142*, 180–186. [[CrossRef](#)] [[PubMed](#)]

6. Henriksen-Lacey, M.; Bramwell, V.; Perrie, Y. Radiolabelling of Antigen and Liposomes for Vaccine Biodistribution Studies. *Pharmaceutics* **2010**, *2*, 91–104. [[CrossRef](#)] [[PubMed](#)]
7. Henriksen-Lacey, M.; Christensen, D.; Bramwell, V.W.; Lindenstrøm, T.; Agger, E.M.; Andersen, P.; Perrie, Y. Liposomal cationic charge and antigen adsorption are important properties for the efficient deposition of antigen at the injection site and ability of the vaccine to induce a CMI response. *J. Control. Release* **2010**, *145*, 102–108. [[CrossRef](#)] [[PubMed](#)]
8. Henriksen-Lacey, M.; Devitt, A.; Perrie, Y. The vesicle size of DDA:TDB liposomal adjuvants plays a role in the cell-mediated immune response but has no significant effect on antibody production. *J. Control. Release* **2011**, *154*, 131–137. [[CrossRef](#)] [[PubMed](#)]
9. Kaur, R.; Bramwell, V.W.; Kirby, D.J.; Perrie, Y. Manipulation of the surface pegylation in combination with reduced vesicle size of cationic liposomal adjuvants modifies their clearance kinetics from the injection site, and the rate and type of T cell response. *J. Control. Release* **2012**, *164*, 331–337. [[CrossRef](#)] [[PubMed](#)]
10. Kaur, R.; Bramwell, V.W.; Kirby, D.J.; Perrie, Y. Pegylation of DDA:TDB liposomal adjuvants reduces the vaccine depot effect and alters the Th1/Th2 immune responses. *J. Control. Release* **2012**, *158*, 72–77. [[CrossRef](#)] [[PubMed](#)]
11. Baxter, L.T.; Zhu, H.; Mackensen, D.G.; Jain, R.K. Physiologically based pharmacokinetic model for specific and nonspecific monoclonal antibodies and fragments in normal tissues and human tumor xenografts in nude mice. *Cancer Res.* **1994**, *54*, 1517–1528. [[PubMed](#)]
12. Chetty, M.; Li, L.; Rose, R.; Machavaram, K.; Jamei, M.; Rostami-Hodjegan, A.; Gardner, I. Prediction of the Pharmacokinetics, Pharmacodynamics, and Efficacy of a Monoclonal Antibody, Using a Physiologically Based Pharmacokinetic FcRn Model. *Front. Immunol.* **2015**, *5*. [[CrossRef](#)] [[PubMed](#)]
13. Garg, A.; Balthasar, J.P. Physiologically-based pharmacokinetic (PBPK) model to predict IgG tissue kinetics in wild-type and FcRn-knockout mice. *J. Pharmacokinet. Pharmacodyn.* **2007**, *34*, 687–709. [[CrossRef](#)] [[PubMed](#)]
14. Glassman, P.M.; Chen, Y.; Balthasar, J.P. Scale-up of a physiologically-based pharmacokinetic model to predict the disposition of monoclonal antibodies in monkeys. *J. Pharmacokinet. Pharmacodyn.* **2015**, *42*, 527–540. [[CrossRef](#)] [[PubMed](#)]
15. Li, L.; Gardner, I.; Dostalek, M.; Jamei, M. Simulation of monoclonal antibody pharmacokinetics in humans using a minimal physiologically based model. *AAPS J.* **2014**, *16*, 1097–1109. [[CrossRef](#)] [[PubMed](#)]
16. Mould, D.R.; Sweeney, K.R. The pharmacokinetics and pharmacodynamics of monoclonal antibodies—Mechanistic modeling applied to drug development. *Curr. Opin. Drug Discov. Dev.* **2007**, *10*, 84–96.
17. Wang, J.; Iyer, S.; Fielder, P.J.; Davis, J.D.; Deng, R. Projecting human pharmacokinetics of monoclonal antibodies from nonclinical data: Comparative evaluation of prediction approaches in early drug development. *Biopharm. Drug Dispos.* **2015**, *37*, 51–56. [[CrossRef](#)] [[PubMed](#)]
18. Van Dissel, J.T.; Arend, S.M.; Prins, C.; Bang, P.; Tingskov, P.N.; Lingnau, K.; Nouta, J.; Klein, M.R.; Rosenkrands, I.; Ottenhoff, T.H.M.; et al. Ag85B–ESAT-6 adjuvanted with IC31<sup>®</sup> promotes strong and long-lived Mycobacterium tuberculosis specific T cell responses in naïve human volunteers. *Vaccine* **2010**, *28*, 3571–3581. [[CrossRef](#)] [[PubMed](#)]
19. Reither, K.; Katsoulis, L.; Beattie, T.; Gardiner, N.; Lenz, N.; Said, K.; Mfinanga, E.; Pohl, C.; Fielding, K.L.; Jeffery, H.; et al. Safety and immunogenicity of H1/IC31(R), an adjuvanted TB subunit vaccine, in HIV-infected adults with CD4<sup>+</sup> lymphocyte counts greater than 350 cells/mm<sup>3</sup>: A phase II, multi-centre, double-blind, randomized, placebo-controlled trial. *PLoS ONE* **2014**, *9*, e114602. [[CrossRef](#)] [[PubMed](#)]
20. Kaur, R.; Henriksen-Lacey, M.; Wilkhu, J.; Devitt, A.; Christensen, D.; Perrie, Y. Effect of Incorporating Cholesterol into DDA:TDB Liposomal Adjuvants on Bilayer Properties, Biodistribution, and Immune Responses. *Mol. Pharm.* **2014**, *11*, 197–207. [[CrossRef](#)] [[PubMed](#)]
21. Milicic, A.; Kaur, R.; Reyes-Sandoval, A.; Tang, C.-K.; Honeycutt, J.; Perrie, Y.; Hill, A.V.S. Small Cationic DDA:TDB Liposomes as Protein Vaccine Adjuvants Obviate the Need for TLR Agonists in Inducing Cellular and Humoral Responses. *PLoS ONE* **2012**, *7*, e34255. [[CrossRef](#)] [[PubMed](#)]
22. Perrie, Y.; Kastner, E.; Kaur, R.; Wilkinson, A.; Ingham, A.J. A case-study investigating the physicochemical characteristics that dictate the function of a liposomal adjuvant. *Hum. Vaccines Immunother.* **2013**, *9*, 1374–1381. [[CrossRef](#)] [[PubMed](#)]
23. Brown, R.P.; Delp, M.D.; Lindstedt, S.L.; Rhomberg, L.R.; Beliles, R.P. Physiological parameter values for physiologically based pharmacokinetic models. *Toxicol. Ind. Health* **1997**, *13*, 407–484. [[CrossRef](#)] [[PubMed](#)]

24. Shah, D.K.; Betts, A.M. Towards a platform PBPK model to characterize the plasma and tissue disposition of monoclonal antibodies in preclinical species and human. *J. Pharmacokinet. Pharmacodyn.* **2011**, *39*, 67–86. [[CrossRef](#)] [[PubMed](#)]
25. Tegenge, M.A.; Mitkus, R.J. A physiologically-based pharmacokinetic (PBPK) model of squalene-containing adjuvant in human vaccines. *J. Pharmacokinet. Pharmacodyn.* **2013**, *40*, 545–556. [[CrossRef](#)] [[PubMed](#)]
26. Leamy, V.L.; Martin, T.; Mahajan, R.; Vilalta, A.; Rusalov, D.; Hartikka, J.; Bozoukova, V.; Hall, K.D.; Morrow, J.; Rolland, A.P.; et al. Comparison of rabbit and mouse models for persistence analysis of plasmid-based vaccines. *Hum. Vaccines* **2006**, *2*, 113–118. [[CrossRef](#)]
27. Hay, J.B.; Hobbs, B.B. The flow of blood to lymph nodes and its relation to lymphocyte traffic and the immune response. *J. Exp. Med.* **1977**, *145*, 31–44. [[CrossRef](#)] [[PubMed](#)]
28. Zhang, Q.; Lu, Y.; Proulx, S.T.; Guo, R.; Yao, Z.; Schwarz, E.M.; Boyce, B.F.; Xing, L. Increased lymphangiogenesis in joints of mice with inflammatory arthritis. *Arthritis Res. Ther.* **2007**, *9*, R118. [[CrossRef](#)] [[PubMed](#)]
29. Michel, C.C. The investigation of capillary permeability in single vessels. *Acta Physiol. Scand. Suppl.* **1979**, *463*, 67–74. [[PubMed](#)]
30. Pappenheimer, J.R. Passage of molecules through capillary walls. *Physiol. Rev.* **1953**, *33*, 387–423. [[PubMed](#)]
31. Sarin, H. Physiologic upper limits of pore size of different blood capillary types and another perspective on the dual pore theory of microvascular permeability. *J. Angiogenes. Res.* **2010**, *2*, 14. [[CrossRef](#)] [[PubMed](#)]
32. Wasserman, K.; Mayerson, H.S. Dynamics of Lymph and Plasma Protein Exchange. *Cardiologia* **1952**, *21*, 296–307. [[CrossRef](#)] [[PubMed](#)]
33. Rodgers, T.; Leahy, D.; Rowland, M. Physiologically based pharmacokinetic modeling 1: Predicting the tissue distribution of moderate-to-strong bases. *J. Pharm. Sci.* **2007**, *96*, 3151–3152. [[CrossRef](#)]
34. Rodgers, T.; Rowland, M. Physiologically-based Pharmacokinetic Modeling 2: Predicting the tissue distribution of acids, very weak bases, neutrals and zwitterions. *J. Pharm. Sci.* **2006**, *95*, 1238–1257. [[CrossRef](#)] [[PubMed](#)]



© 2017 by the authors. Licensee MDPI, Basel, Switzerland. This article is an open access article distributed under the terms and conditions of the Creative Commons Attribution (CC BY) license (<http://creativecommons.org/licenses/by/4.0/>).